catalysts

MDPI

*Article*

# Stability of Ruthenium/Carbon Catalytic Materials during Operation in Carbon Monoxide Methanation Process

**Elżbieta Truszkiewicz [1,*], Klaudia Latoszek [1], Milena Ojrzyńska [2], Andrzej Ostrowski [1] and Leszek Kępiński [3]**

[1] Faculty of Chemistry, Warsaw University of Technology, Noakowskiego 3, 00-664 Warsaw, Poland; klaudia.latoszek.stud@pw.edu.pl (K.L.); andrzej.ostrowski@pw.edu.pl (A.O.)
[2] Faculty of Physics, Warsaw University of Technology, Koszykowa 75, 00-662 Warsaw, Poland; milena.ojrzynska@pw.edu.pl
[3] Institute of Low Temperature and Structure Research, Polish Academy of Sciences, Okólna 2, 50-950 Wrocław, Poland; l.kepinski@intibs.pl
* Correspondence: elzbieta.truszkiewicz@pw.edu.pl; Tel.: +48-22-2341786

**Abstract:** The stable activity of catalysts is an important characteristic, which determines their suitability for industrial applications. The purpose of this study was to investigate the stability of ruthenium systems deposited on carbon under conditions simulating long-term operation in CO methanation. Two series of Ru/carbon catalysts were prepared and studied during CO methanation in a hydrogen-rich gas stream. Two graphitized carbons substantially differing in their surface area (23 and 1457 $m^2/g$) were used as supports, and Ru loadings of 3 and 6 wt.% were applied. The stability of Ru/C catalysts was examined in a 240 h time-on-stream test. The samples were characterized by CO chemisorption, XRD, TEM, Raman spectroscopy, TG–MS studies and CO-TPD. The stability of the catalysts over 240 h in the CO + $H_2$ mixture depended on the support type and Ru loading. The highest CO conversion and increased activity was observed for both catalysts with Ru dispersion above 80%. The tested systems were also resistant to carbon deposition. Interestingly, a similar level of activity was obtained for 3 wt.% Ru supported on the low surface area carbon. It is presumed that the similar activity observed for systems with such different ruthenium dispersion is related to the presence of active sites of different strength and structure on the surface of both small and large Ru particles.

**Keywords:** ruthenium catalyst; carbon support; long-term stability; CO methanation



**Citation:** Truszkiewicz, E.; Latoszek, K.; Ojrzyńska, M.; Ostrowski, A.; Kępiński, L. Stability of Ruthenium/Carbon Catalytic Materials during Operation in Carbon Monoxide Methanation Process. *Catalysts* **2023**, *13*, 1518. https://doi.org/10.3390/catal13121518

Academic Editor: Enrique García-Bordejé

Received: 16 November 2023
Revised: 12 December 2023
Accepted: 15 December 2023
Published: 18 December 2023



## 1. Introduction

The stability of catalysts, understood as the maintenance of a satisfactory level of activity over a long period of operation, is one of the key factors determining their application potential in industry. In some large-scale chemical processes, for example in ammonia synthesis, the difficulties associated with the replacement of a catalyst in an industrial plant are so great that catalysts are sought to work stably for 10 years or more [1]. For these reasons, research on the behavior of catalysts over longer operating times is constantly being undertaken and expanded with new scientific groups [2–6]. According to [1], several mechanisms of solid catalyst deactivation can be grouped into six intrinsic mechanisms of catalyst decay: (1) poisoning, (2) fouling, (3) thermal degradation, (4) vapor compound formation and/or leaching accompanied by transport from the catalyst surface or particle, (5) vapor–solid and/or solid–solid reactions, and (6) attrition/crushing. An important group of contacts exposed to deactivation due to carbon deposition are catalysts operating in streams containing carbon compounds. Generally, two main forms of carbon deposit can be indicated [7]. Coke, which encapsulates a part of the surface, is produced from reaction intermediates by subsequent condensation and polymerization [7]. On the other hand, the dissociation of small coke precursors (CO, $CH_4$ or other light $C_xH_y$) results in the formation of atomic carbon and, next, to the formation of filamentous coke [7]. An

example of that latter process is catalytic $CO_x$ methanation [8]. It has applications in the purification of hydrogen-rich streams from trace amounts of carbon oxides in ammonia production facilities [9,10] and in hydrogen purification for other applications, such as fuel cells [11,12].

The catalyst commonly used in industrial methanation of carbon monoxide is nickel deposited on $Al_2O_3$ [13,14]. However, ruthenium systems deposited on various supports show high activity in this process [3,14–17]. A number of papers have also been devoted to changes in the activity of ruthenium systems over time [4,18]. Zhang [19] reported the excellent stability of 2 wt.% $Ru/Al_2O_3$ catalysts within 4320 min on stream at 320 °C, with the conversion of CO above 97% (the applied feed composition was $CO/H_2 = 1/3$). Chen [4] described the catalytic activity of three 1.9 wt.% $Ru/TiO_2$ catalysts, obtained using supports with different surface structures. Their stability was evaluated in a medium CO content reformate gas (6000 ppm CO,15.5% $CO_2$, 3% $N_2$ and $H_2$ balance) at 190 °C for 950 min. For one of them, the Ru mass-normalized reaction rate increased during the first 50 min, but then decreased continuously with time on stream. Two other systems exhibited much longer activation phases, reaching the highest activity and stability after 350 min [4]. The authors [4] revealed that supports with a larger number of surface defects stabilize highly dispersed, flat Ru NPs. In contrast, Ru nanoparticles supported on more ordered materials lack this stabilization and undergo gradual shape changes during selective CO methanation. The authors [4] associate this effect with smaller electronic modifications to the surface of Ru atoms, resulting in the continuous, slow deactivation of the catalyst supported on $TiO_2$ with a more ordered structure. Similar conclusions were reported by Eckle [16]. Although ruthenium catalysts supported on carbon materials exhibit promising properties [20–23], there is a lack of reports concerning the thermostability of ruthenium systems supported on carbon carriers. A La-doped 10 wt.% Ru/C1 catalyst exhibited stable activity during 72 h of overheating at 300 °C, which indicates satisfactory thermal resistance of La–Ru/carbon systems [23].

The purpose of the present work was to check the activity of ruthenium catalysts over a longer period of time. Moreover, we studied the effect of the carbon support type, the ruthenium loading and its dispersion on the thermal stability of the modified carbon-supported ruthenium catalysts. The term "thermal stability" (thermoresistance) is used here as the ability of the system to maintain its activity during a long period of operation under reaction conditions.

## 2. Results and Discussion

### *2.1. Evaluation of the Catalytic Performance*

All the prepared catalysts were subjected to stability tests to determine the effect of the carbon support and ruthenium loading on the activity of the catalysts over a long period of time. The catalytic tests on the first day were preceded by an initial reduction (activation) in hydrogen. All the catalytic tests were performed at three temperatures (270–240–220 °C) in a $CO + H_2$ gas mixture (5000 ppm CO in $H_2$, 80 $cm^3$/min). After the last analysis, the temperature was raised to 300 °C and the same composition of the inlet gas stream was maintained overnight in order to simulate overheating of the catalyst during long-term operation. Next, the reactor was cooled back to 270 °C and the whole procedure of testing and overheating was repeated. The main product of CO hydrogenation over Ru/C catalysts was $CH_4$, with trace amounts of $CO_2$ and $C_2H_4$ detected. The activity of the catalysts was expressed in terms of reaction rates normalized to the same Ru content in the sample to compare the activity of the samples differing in their composition. The reaction rates obtained in the time-on-stream tests are presented in Figure 1.

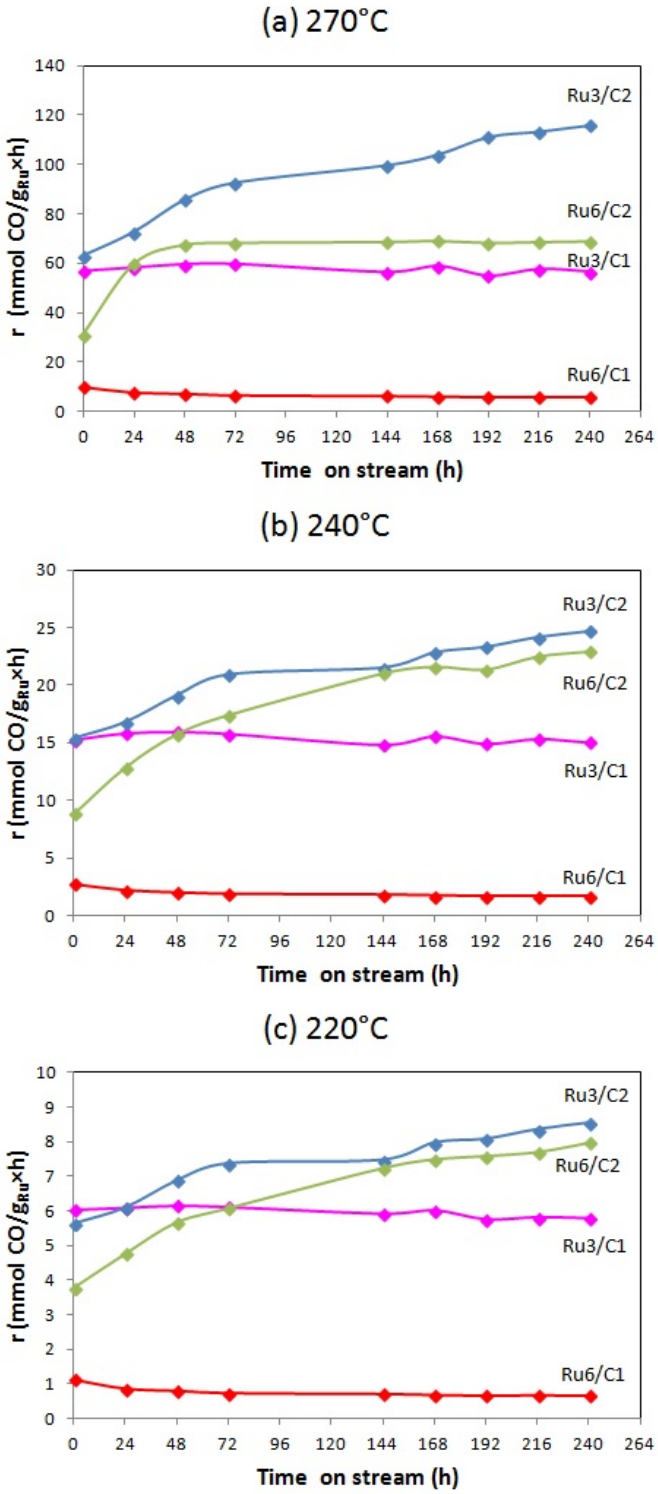


**Figure 1.** Time-on-stream performance of the Ru/carbon catalysts at: (**a**) 270 °C, (**b**) 240 °C and (**c**) 220 °C. Measurement conditions: 0.1 MPa, 5000 ppm CO in CO + $H_2$ mixture, 80 $cm^3$/min. Overheating conditions: 300 °C, 0.1 MPa, 5000 ppm CO in CO + $H_2$ mixture, 80 $cm^3$/min (for 24 h or 72 h during the weekend).

The results presented in Figure 1 clearly indicate that the behavior of the catalysts during the long–term tests depends on their composition, support type and active phase loading. Catalysts based on the C1 support were generally less active than their C2–supported counterparts. Moreover, when comparing samples supported on the same

carrier, we observed that those with a lower ruthenium loading (3 wt.%) were more active than those containing 6 wt.% of ruthenium.

In the case of C1–based catalysts, the initial activity of the sample with the lower ruthenium loading (3 wt.%) was more than 5–6 times higher, depending on the test temperature, than that obtained for Ru6/C1. This difference increased with time. Sample Ru3/C1 (Figure 1) showed almost constant reaction rates at all temperatures and appeared to be strongly resistant to overheating. It can be stated that after an initial drop it achieved a stable activity level. Only a slight, less than 5%, decrease in the reaction rate was observed after 240 h compared to the initial value, i.e., after a reduction. For Ru6/C1, regardless of the temperature, a noticeable decrease in activity was observed over time, to a level of 60% of the initial value. The levels of CO conversion registered for C1–supported catalysts during 240 h of stability tests exhibited similar trends as the reaction rates described above. The highest values of CO conversion achieved at 270 °C were about 40% and 14% for Ru3/C1 and Ru6/C1, respectively (Figure S1a).

In contrast, no activity loss was noted during the long–term activity tests on the C2–supported catalysts. The sample Ru3/C2 showed higher reaction rates than Ru6/C2. Both samples exhibited a constant increase in activity over time (Figure 1). The only exception, i.e., the stabilization of the reaction rate reached after 48 h of the stability test, was observed for the catalyst Ru6/C2 at 270 °C (Figure 1a). This is due to the fact that a CO conversion of almost 100% was reached for Ru6/C2 (Figure S1a). When considering the activity related to the weight of ruthenium in the catalyst, the advantage of the Ru3/C2 catalyst over the Ru6/C2 sample observed at 270 °C (Figure 1a) disappeared at lower temperatures (Figure 1b,c). The temperature range of 240–220 °C seems to be more reliable for comparison due to the lower CO conversion values achieved (Figure S1b,c). Therefore, it is inferred that both C2–supported catalysts exhibited similar catalytic activity in the studied reaction. It should also be noted that the observed activity trend is similar to that reported by [4] for the $Ru/TiO_2$ catalyst.

The possible reasons for the observed catalytic behavior of Ru/carbon catalysts will be discussed further in light of the presented physicochemical characteristics. In the case of carbon–supported Ru, it was shown that a reduction in hydrogen at 300 °C ensures the complete reduction of the Ru system prepared from the chloride precursor ($RuCl_3$) [24]. An increase in the activity of the Ru/C2 catalysts with time on stream may be attributed to the restructurization of small Ru particles (ordering of the crystal structure, faceting) to be more suitable for the structure–sensitive methanation reaction [25]. It may also be influenced by the functional groups on the surface of modified carbon materials [26]. It is generally known that they have a significant influence on the ruthenium reduction/oxidation state and the stabilization of its active, reduced form [27].

To compare the present activity results with other ruthenium catalysts supported on carbon materials, let us refer to Kumi [22]. Catalysts containing 5 wt.% of Ru supported on different carbon spheres were tested in a mixture of 1% CO and 89% $H_2$ (balance $N_2$), in the temperature range between 100 and 360 °C (1 g sample) [22]. All the catalysts presented by Kumi [22] completely converted CO within a temperature range of 240–300 °C. In the case of Ru6/C2, complete CO conversion was reached at 270 °C (Figure S1b). However, it should be noted that the weight of the catalyst used in the present study was four times lower than that described in [22]. Therefore, we expect that a comparable weight of the Ru6/C2 catalyst would yield 100% conversion at a lower temperature. Moreover, the CO conversion levels obtained in this work (Figure S1) are higher than those previously reported by our team [23]. The values of the apparent activation energy for the studied samples were estimated on the basis of data collected on the first day of the stability tests. The obtained values (determination error ± 2%) were as follows: 100 kJ/mol for Ru3/C1, 97 kJ/mol for Ru6/C1, 108 kJ/mol for Ru3/C2 and 94 kJ/mol for Ru6/C2. These results are very similar. However, the lowest activation energy was obtained for the Ru6/C2 sample, for which the highest CO conversions were achieved (Figure S1). The activation energy

values estimated for the studied catalysts are in good agreement with the data previously published on supported ruthenium systems during $CO_x$ methanation [17,28,29].

### 2.2. CO Chemisorption

To determine the ruthenium dispersion (FE—fraction of atoms exposed) in fresh and spent Ru/carbon catalysts, we performed static measurements of the CO chemisorption. The amounts of CO adsorbed on the surfaces of the catalysts was used for the FE calculations. Next, using equations in the literature [30], the average sizes of the ruthenium particles in the catalysts ($d_{Ru}$) were calculated, assuming CO:$Ru_S$ = 0.6:1 adsorption stoichiometry [28]. The obtained FE and $d_{Ru}$ values are presented in Table 1.

**Table 1.** CO chemisorption data on the Ru/C catalysts: fresh and spent.

| Catalyst | FE (%) | | $d_{Ru}$ (nm) | |
|---|---|---|---|---|
| | Fresh | Spent | Fresh | Spent |
| Ru3/C1 | 2.3 | 1.5 | 57 | 87 |
| Ru6/C1 | 0.94 | 1.2 | 140 | 108 |
| Ru3/C2 | 91 | 90 | 1.5 | 1.5 |
| Ru6/C2 | 84 | 91 | 1.6 | 1.5 |

Two different trends in the change of the sample structure, depending on the ruthenium content, were observed (Table 1). Fresh catalysts supported on carbon C1, characterized by a low specific surface area, exhibited low dispersion of ruthenium (FE = 1–2% for fresh samples, Table 1) and quite large crystallite sizes ($d_{Ru}$ > 50 nm, Table 1), despite the relatively low ruthenium content in the samples. In the case of samples deposited onto the high–surface–area carbon, C2, high dispersion of the active phase was achieved with the same ruthenium contents (3 and 6 wt.%). Better metal dispersion on the support with a higher specific surface area is not surprising [25].

After the thermal stability tests, a small decrease in the ruthenium dispersion in the sample Ru3/C1s was noted (Table 1). Such a phenomenon is common in the literature and is associated with the sintering of small particles in the active phase [1]. Interestingly, for samples with 6 wt.% ruthenium content, the opposite effect was obtained: increased ruthenium dispersion was observed in the spent catalysts compared to fresh samples (Table 1). This effect may be attributed to surface reconstruction, as it was observed for the iron catalyst during CO hydrogenation [31].

By analyzing the obtained chemisorption results (Table 1) with the results from the activity tests (Figure 1), it can be concluded that changes in the size of the Ru crystallites during operation do not correlate directly with the changes in the activity over time. The samples containing initially smaller crystallites in the active phase showed increasing activity in the CO methanation over time (Figure 1). However, it should be noted that the Ru3/C1 catalyst was not much more inferior to them in terms of the reaction rate, especially compared to Ru6/C2 (Figure 1a,c). The literature reports indicate an optimal size of ruthenium particles, guaranteeing the best properties in the catalytic hydrogenation of CO to methane [26,32–34]. It seems that in our case, the size of the crystallites in the active phase is not the most important and only factor determining the activity of the system, despite the fact that it causes different electronic properties in very small Ru nanoparticles compared to larger ones [16].

### 2.3. XRPD

In order to determine the phase composition of the catalysts, X–ray diffraction studies were performed. The diffraction patterns of the supports used are shown in Figure S2. They are typical for activated carbons. No particular differences were observed between C1 and C2. Characteristic signals of graphite and turbostratic carbon [35,36] can be seen, which indicates a partial ordering in the crystalline structure of the carriers.

The diffraction patterns of four Ru/carbon catalysts used in this study are presented in Figure 2. The phase composition of the samples was determined based on the PDF card numbers given in Figure 2.

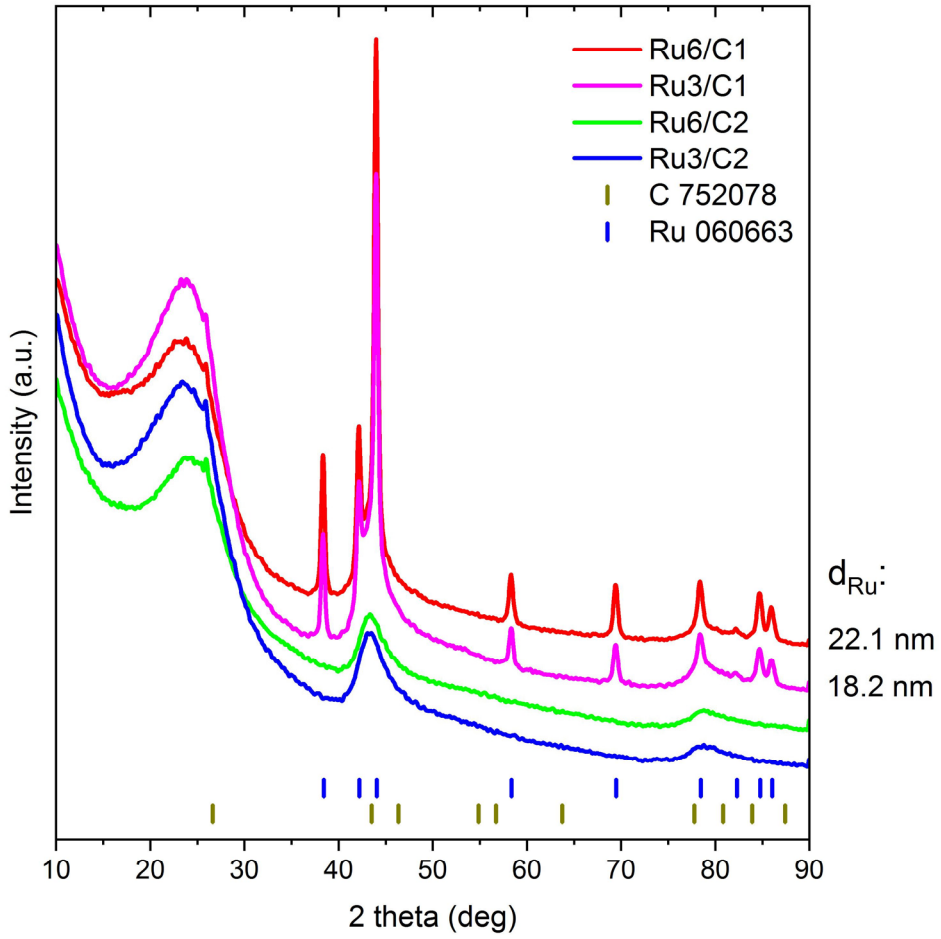


**Figure 2.** XRPD patterns of the fresh ruthenium catalysts; $d_{Ru}$– the average Ru crystallite sizes in Ru/C systems estimated based on XRPD data.

The XRPD patterns for the Ru3/C2 and Ru6/C2 samples do not differ qualitatively from the one shown for the pure C2 (Figure S2). Apart from the signals originating from carbon, no traces of ruthenium can be seen, indicating its high dispersion, which is in agreement with the data shown in Table 1. In the case of the samples deposited on carbon C1, distinctive signals from metallic ruthenium were observed. The Scherrer equation [26] was applied to calculate the average size of the Ru crystallites in these catalysts. The obtained $d_{Ru}$ values are shown in Figure 2. As can be seen, they are significantly lower than those determined by CO chemisorption (Table 1). A more extensive discussion on the reasons for the discrepancies between the results estimating the size of the metal crystallites conducted using different techniques can be found in [25]. It is presumed that in the samples deposited on support C1, ruthenium forms polycrystalline Ru particles. In this case, XRD showed the sizes of the coherent scattering regions (Figure 2), whereas chemisorption characterized the particle sizes. Nevertheless, it is worth noting that a larger $d_{Ru}$ value was also obtained in the case of the sample with higher active phase content.

### *2.4. TEM*

Observations were conducted using a transmission electron microscope for all four catalysts in fresh and spent forms. The average ruthenium particle sizes (d Ru), calculated from the particle size distributions obtained from the TEM images, are included in the

proper figures. The error in the determination of the d Ru parameter is also presented. A selection of the images obtained for C1–supported samples is shown in Figures 3 and 4.

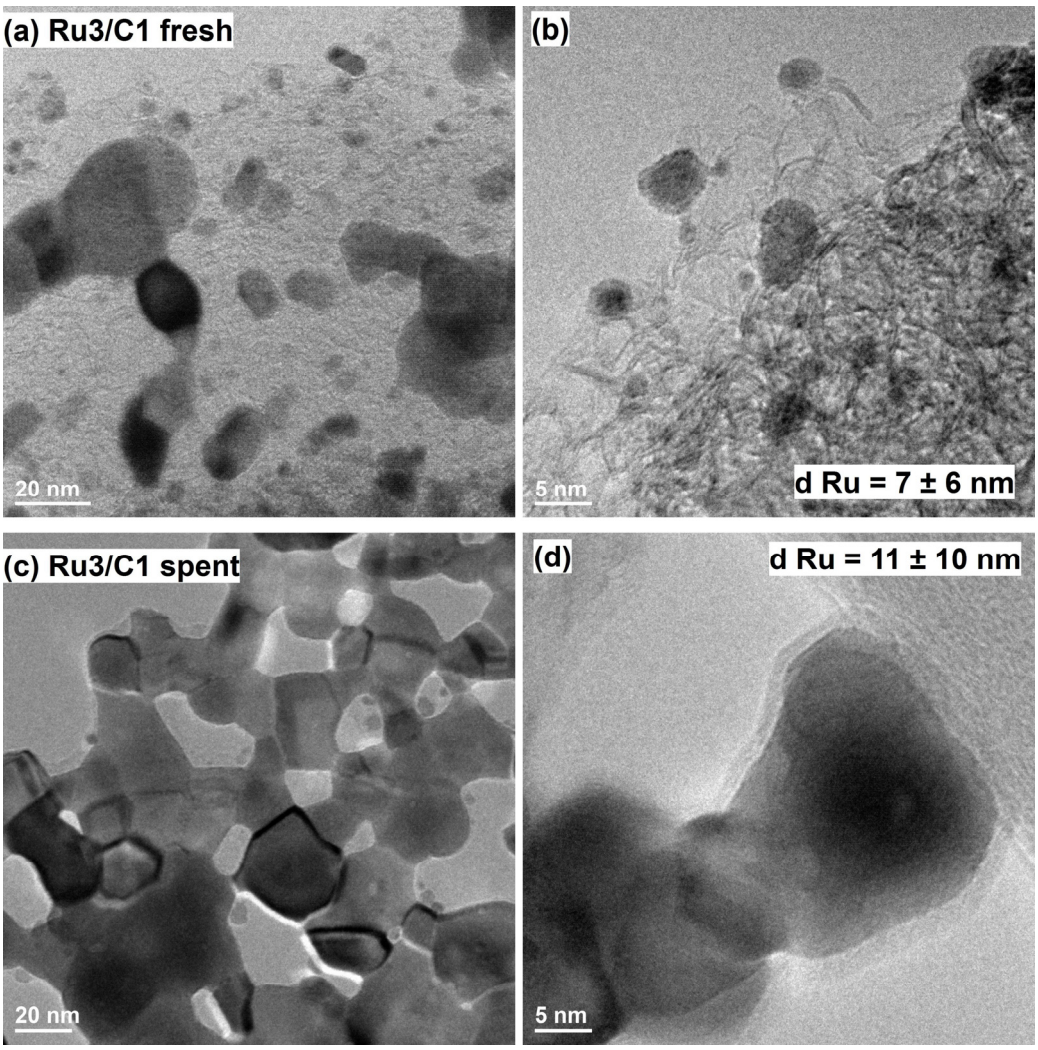


**Figure 3.** TEM images of Ru3/C1 catalyst (**a**,**b**) fresh and (**c**,**d**) spent.

The TEM images obtained for the Ru3/C1 and Ru6/C1 catalysts show their high heterogeneity (Figures 3 and 4). The size distributions of the Ru particles on the carbon support in fresh materials (Figures 3a,b and 4a,b) are very broad. This is due to the small specific surface area of the carrier C1. For this reason, estimating the d Ru is fraught with a substantial level of error and should be treated qualitatively rather than quantitatively. The values for Ru3/C1 and Ru6/C1 were estimated at 7 nm and 19 nm, respectively (Figures 3b and 4b). It appears that much of the ruthenium has formed large aggregates of particles. Ru nanocrystallites in such aggregates are interconnected, which lowers the surface area available for gaseous reactants. These results fit well in the picture obtained from the chemisorption measurements (Table 1). Titration of the ruthenium surface using adsorbed CO led to the determination of large crystallite sizes. Despite the substantial estimation error, the values obtained from the TEM analysis are in good agreement with those estimated from the X–ray diffractograms for C1–supported samples (Figure 2). It is also clear that the average size of the ruthenium particles in the Ru6/C1 sample is about twice that of the Ru3/C1 sample, analogous to what was observed in the chemisorption studies (Table 1). In both fresh Ru3/C1 and Ru6/C1 catalysts (Figures 3 and 4), the surface of large Ru particles is clean or covered with a thin layer of its amorphous oxide, which

becomes thicker with the decreasing ruthenium particle size. A similar effect was observed in [26].

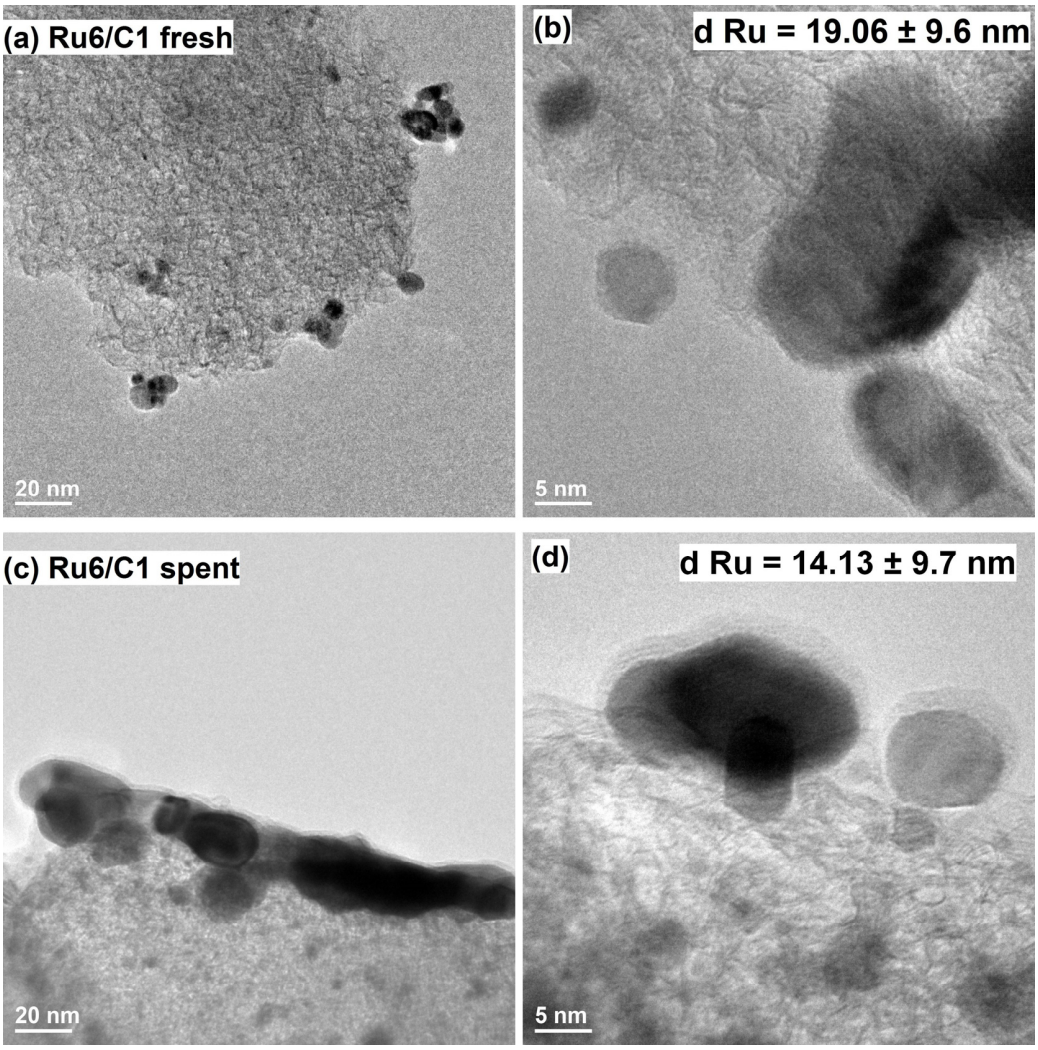


**Figure 4.** TEM images of Ru6/C1 catalyst (**a**,**b**) fresh and (**c**,**d**) spent.

No large changes in morphology were observed for the spent Ru3/C1 and Ru6/C1 catalysts (Figures 3c,d and 4c,d) compared to the fresh samples. The interconnected particles of the active phase are clearly visible. The average d Ru sizes were estimated at 11 nm and 14 nm for Ru3/C1 and Ru6/C1, respectively. The observed trends in the changes in the average size of the Ru particles due to the long operation were similar to those obtained for these catalysts as a result of the chemisorption studies (Table 1). Thus, it seems that, despite the imprecision of the estimation, the d Ru values estimated on the basis of the TEM data reflect the trends in the structural changes of the active phase crystallites during the catalyst operation well. In our case, the HRTEM data are the most reliable, because of the broad particle size distribution and observed agglomeration of the particles.

The main difference observed for the spent C1–supported catalysts (Figure 3c,d and Figure 4c,d) is the appearance of an amorphous layer about 1.5–2 nm thick, probably a carbon deposit, on the surface of large Ru particles. Its deposition may be related to a slight decrease in the activity of the catalysts during the thermostability test (Figure 1). No other forms of carbon deposits (e.g., fibers [37]) were observed in the spent catalysts. The structure and nature of the deactivating carbon formed during low–temperature CO methanation has already been the topic of several studies [38–40].

Selected TEM images obtained for the C2–supported catalysts are shown in Figures 5 and 6.

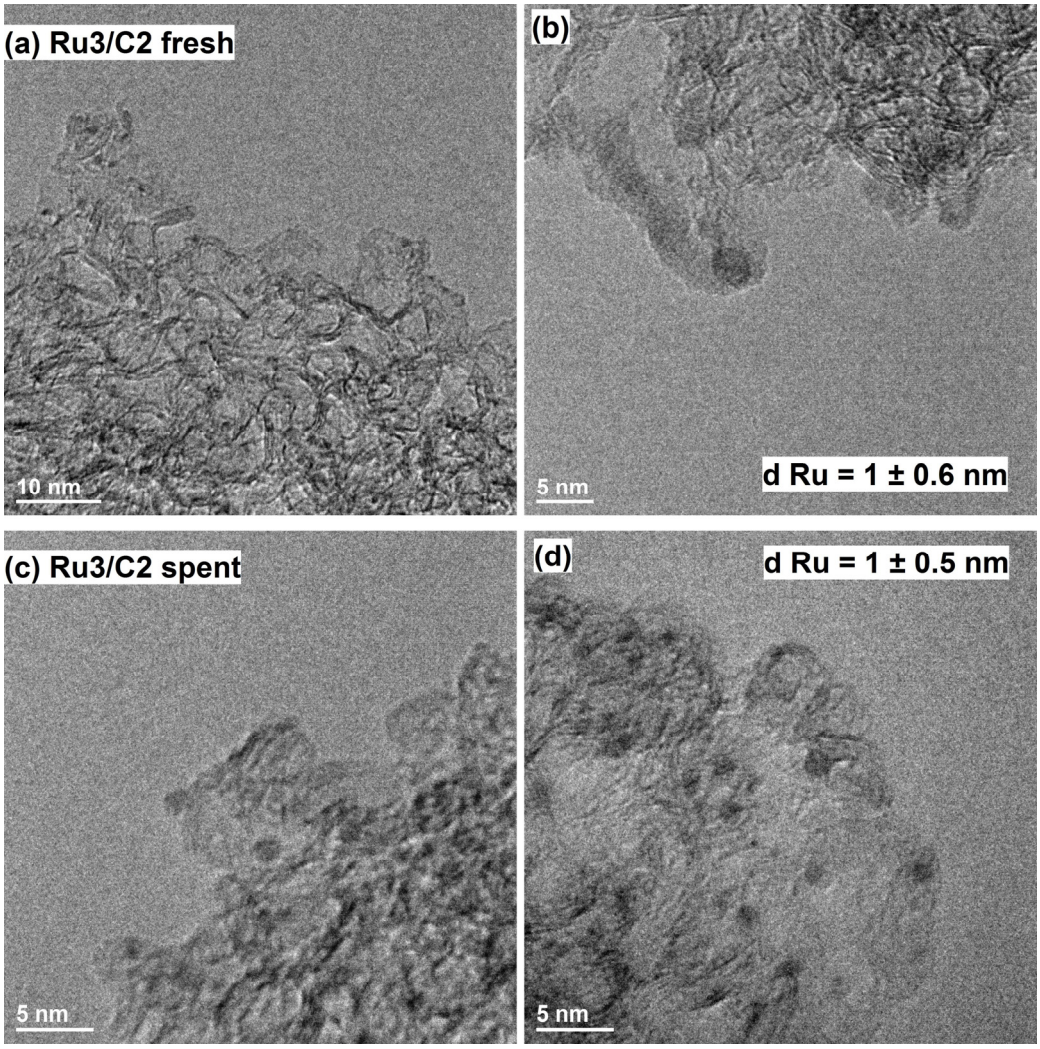


**Figure 5.** TEM images of Ru3/C2 catalyst (**a**,**b**) fresh and (**c**,**d**) spent.

It is clearly visible that the TEM images obtained for the C2–supported ruthenium catalysts significantly differ from those obtained for the C1–supported materials. As presented in Figures 5 and 6, the Ru3/C2 and Ru6/C2 catalysts have a homogeneous structure. The metallic phase nanoparticles are uniformly distributed on the C2 support as individual particles with a narrow size distribution. It cannot be unambiguously determined whether ruthenium is present here in the form of Ru or $RuO_2$. Aggregates of metal particles were not observed. The estimated average d Ru size was 1 nm for both the fresh and spent Ru3/C2 catalyst (Figure 5b,d). In the case of Ru6/C2, the d Ru values estimated for the fresh and spent catalysts were practically the same: 1 nm (Figure 6b,d). Taking into account the error in estimating the d Ru values in TEM studies, it should be assumed that no significant changes in the ruthenium particle sizes occurred during the stability tests on C2–supported catalysts. During the TEM observations performed for the fresh Ru6/C2 catalyst, much larger particles were also observed and identified as metallic ruthenium. This may be the reason for the slightly higher $d_{Ru}$ value estimated from the chemisorption results for the fresh Ru6/C2 in comparison to the spent sample (1.6 nm versus 1.5 nm, Table 1).

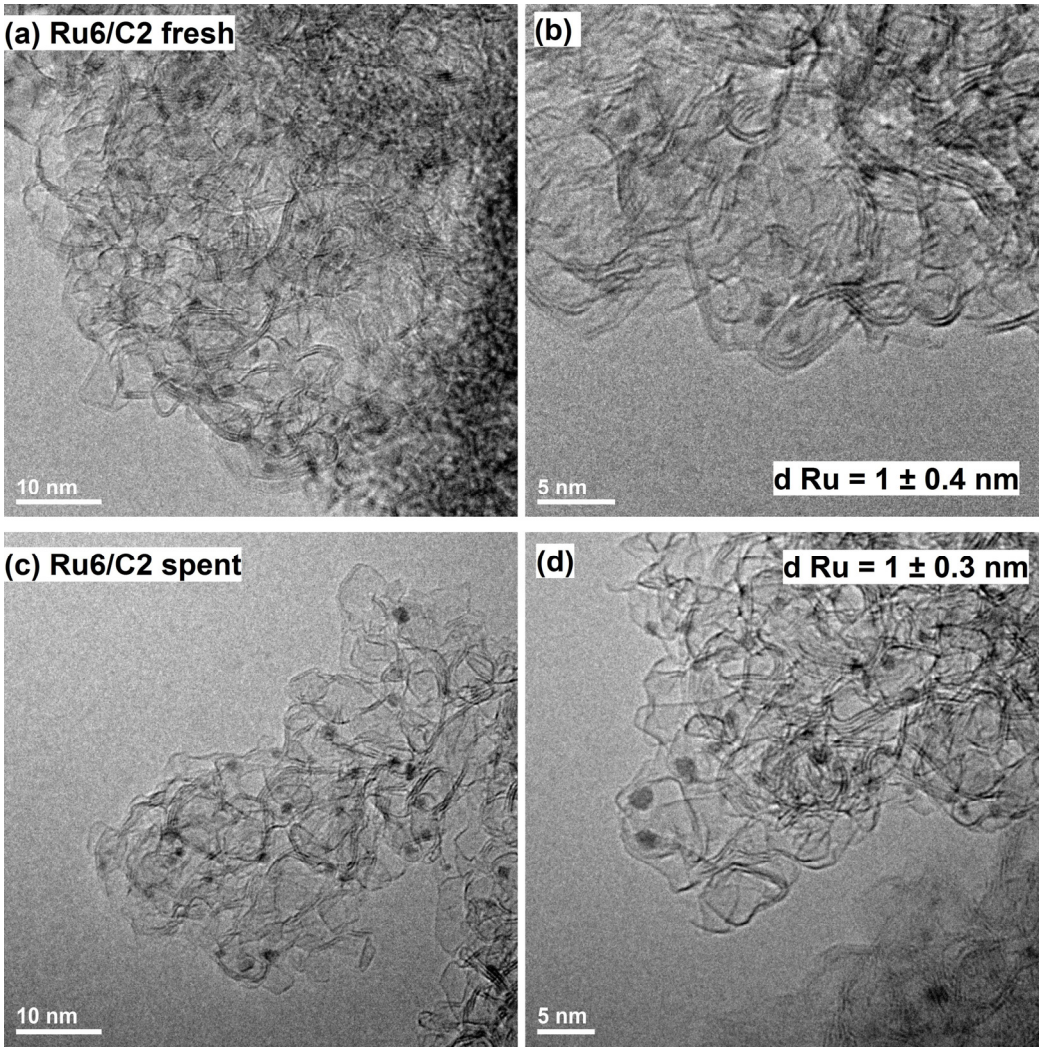


**Figure 6.** TEM images of Ru6/C2 catalyst (**a**,**b**) fresh and (**c**,**d**) spent.

Comparing the fresh samples with the materials after the stability test, no clear differences could be indicated. The metal particles are more visible in the spent catalyst (Figures 5c,d and 6c,d). The reason for that could be, for example, the reduction in the $RuO_x$ species, which are always present on the surface part of the active phase crystallite in the fresh sample, as was observed for the C1–supported catalyst (Figures 3 and 4). A similar effect was observed by Chen [4]. Their XANES data revealed that during the reaction, the content of metallic Ru species in the $Ru/TiO_2$ system increased from 32.0% to 90.0% after 10 min and stayed stable at this level [4]. Another reason could be the slight increase in Ru particle sizes, indicated by the chemisorption data (Table 1). The chemical identification of the composition of these particles was not possible. The reason may be their amorphous structure, resulting, for example, from deeper oxidation. Some Ru particles in the spent Ru6/C2 catalyst had well–developed faces (Figure 6d) and, in this respect, were distinguished from particles in the fresh Ru6/C2 sample (Figure 6a,b). Importantly, no carbon deposits were observed on the surface of the particles in the spent catalysts. However, it should be noted that for such small particles, the presence of a very thin layer may be impossible to detect.

### *2.5. Raman Spectral Analysis*

The Raman patterns for the fresh and spent catalysts were examined to explore the influence of the long–term stability tests on the extent of the structural disorder in the

carbon supports. The corresponding spectra are shown in Figure 7. Two fresh carbon supports were also studied (Figure 7a).

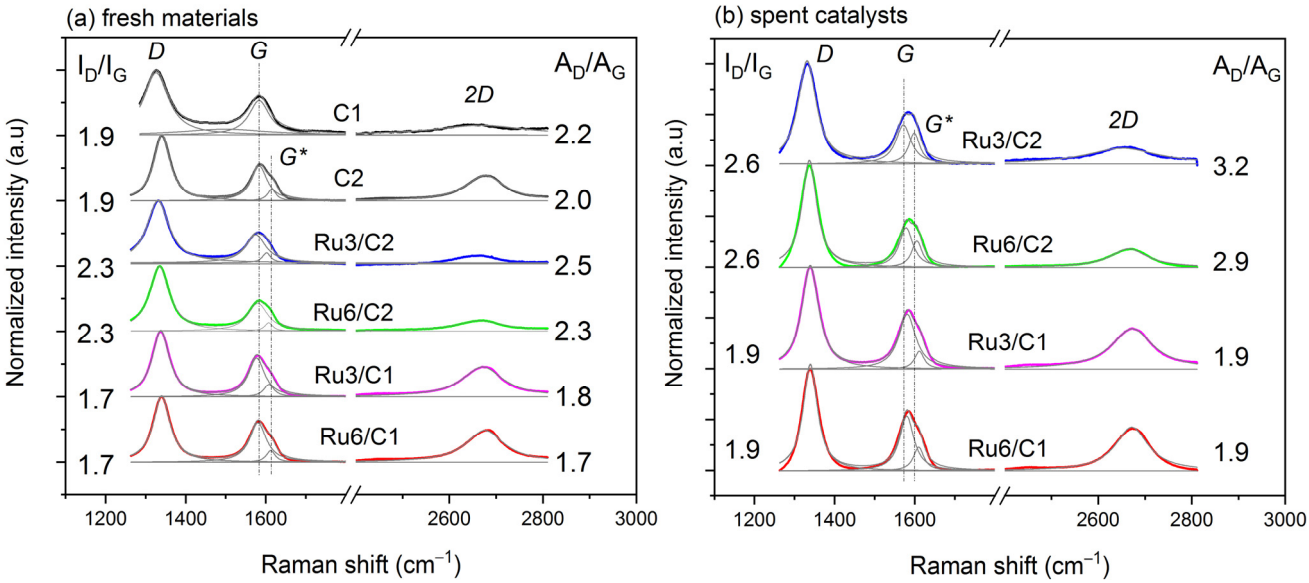


**Figure 7.** Raman spectra of: (**a**) fresh carbon supports and catalysts, (**b**) spent catalysts; the intensity ratio of the D and G bands ($I_D/I_G$) and the area ratio of the D and G bands ($A_D/A_G$) included.

All the obtained Raman spectra contained an intense band at about 1596 cm$^{-1}$ corresponding to the in–plane, involving symmetric stretching vibrations of the C=C sp2 bonds (G band) [36]. This mode does not require the presence of sixfold rings, thus it occurs at all sp2 sites. Two bands associated with the defective structure of the carbon materials were also visible: D band (1330 cm$^{-1}$) and G* band (~1630 cm$^{-1}$) [41]. The D band is a breathing mode in $A_{1g}$ symmetry and its intensity is connected with the presence of sixfold rings. A broad and symmetric 2D peak (~2670 cm$^{-1}$) indicates the turbostratic structuring of the carbon material [36], in agreement with the XRD data (Figure 2).

The introduction of ruthenium on the support surface caused visible changes in the 2D band in both series, but they were of a different nature for C1 and C2 carbons (Figure 7a). This is in line with previous observations by Guo [27], who observed differences in the Raman spectra for ruthenium catalysts supported on multiwalled carbon nanotubes, depending on the type of carrier used [27].

All samples exhibited an intensity ratio ($I_D/I_G$) and area ($A_D/A_G$) under the D and G bands above 1, indicating a high ratio of sp3 to sp2 bonds, as commonly expected in carbon samples. In the case of amorphous carbons with a small cluster diameter (<20 Å), the D mode strength is proportional to the probability of finding a sixfold ring in the cluster. So, in amorphous carbons, developing a D peak can indicate the ordering of sixfold rings [42]. The difference between the ratio of intensities and fields under the profile is due to changes in the full width at half the maximum of the D ($\Gamma_D$) and G ($\Gamma_G$) bands, which depended on the disorder (see Table S1). Broadening and narrowing modes can be associated with changes in the lifetime of phonons, so increasing and decreasing the defect concentration, such as distortion in the bond length and angles, respectively [42]. While the $\Gamma_G$ values are proportional to the disorder, materials with unstrained or defect–free sp2 clusters will exhibit smaller $\Gamma_G$ values [43]. In the case of our samples, changes in the $\Gamma_G$ can also be associated with changes in the G* peak intensity and position. The introduction of ruthenium on the support surface also caused changes in the position of the G peak (ωG), but the differences were very low (up to a few cm$^{-1}$) (see Table S1).

In the case of spent catalysts, there is an obvious increase in the $I_D/I_G$ ratio for all samples (Figure 7b) compared to their fresh counterparts. This may be related not only to

structural changes in the bulk support, but also to the appearance of carbon deposits on the surface of the samples (compare TEM results, Figures 3–6).

### *2.6. TG–MS*

The TG–MS experiments, representing temperature–programmed reduction, were performed over freshly prepared catalysts to examine the resistance to undesired methanation of both carbon supports used for catalyst preparation. Additionally, the effect of ruthenium loading in the sample was examined. It must be mentioned that the modified carbon support itself does not undergo hydrogenation to methane [44]. Figures 8 and 9 show the TG–MS profiles for the catalysts supported on C1 and C2 materials, respectively. The mass spectrometer signals corresponding to water (m/e = 18) and methane (m/e = 15) are also shown.

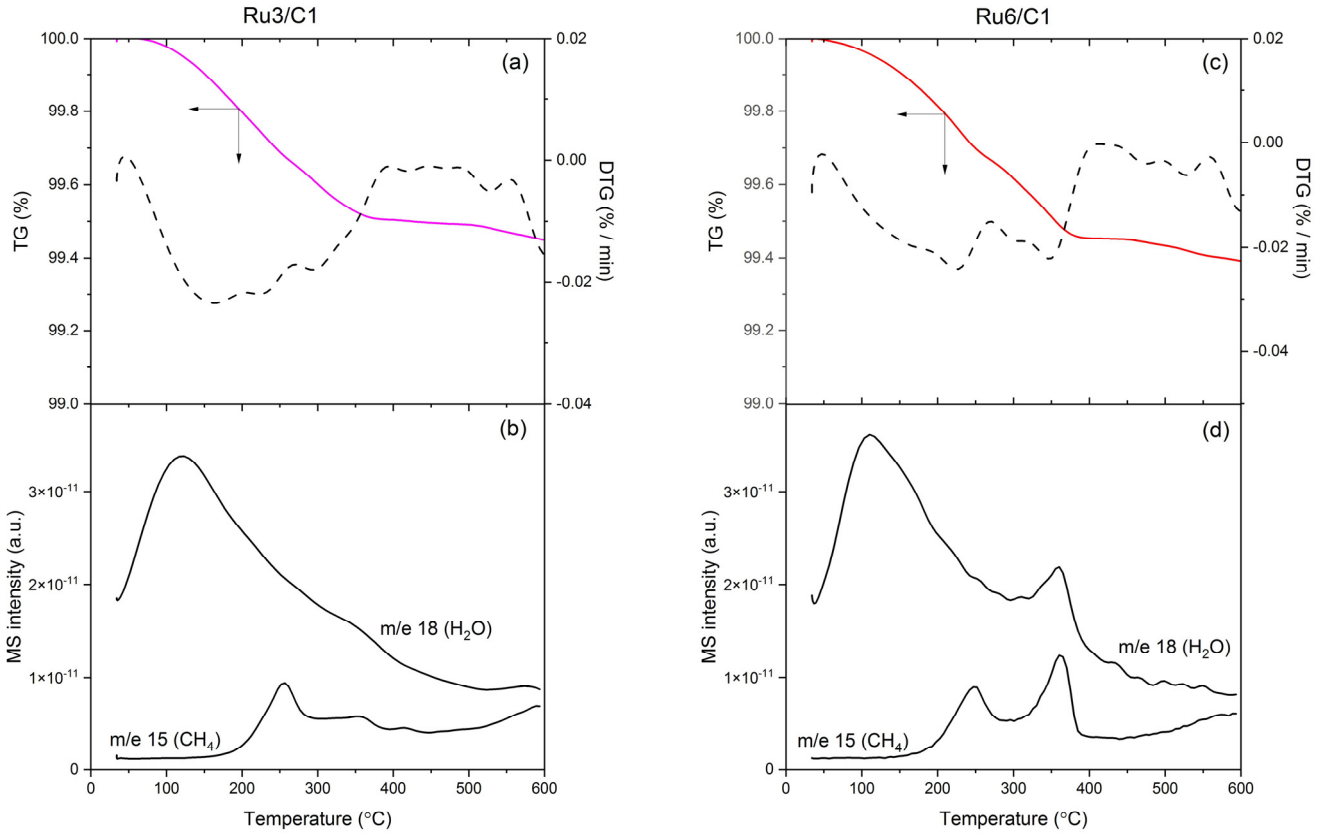


**Figure 8.** TG/DTG–MS profiles of the C1–supported catalysts: (**a**) Ru3/C1 mass loss during heating to 600 °C, (**b**) Ru3/C1 MS signal of water and methane evolution, (**c**) Ru6/C1 mass loss during heating to 600 °C, (**d**) Ru6/C1 MS signal of water and methane evolution.

The course of reduction in the Ru3/C1 and Ru6/C1 samples is similar (Figure 8). The total mass loss does not exceed 0.6% by weight for either of them (Figure 8a,c, TG line). In the temperature range up to 400 °C, the DTG curve indicates two, rather stretched in time, stages of mass loss, accompanied by water release (m/e = 18, Figure 8b,d). Such a drawn–out course of reduction may be indicative of heterogeneous particle sizes in the reducing active phase. This hypothesis is supported by the TEM observations on the Ru3/C1 and Ru6/C1 samples (Figures 3 and 4). The first water signal is very broad, with a maximum temperature of around 100–120 °C. It is related to the evaporation of moisture from the sample, but also to the reduction of the oxide passivation layer on the ruthenium. The second stage of sample reduction takes place at about 360 °C. In the Ru6/C1 sample (Figure 8d), this water signal is more intense than that observed for Ru3/C1 (Figure 8b). This effect is probably related to the reduction in the larger ruthenium particles. Their

contribution to the catalyst is higher for the sample with higher Ru content, as indicated by both the chemisorption results (Table 1) and the TEM observations.

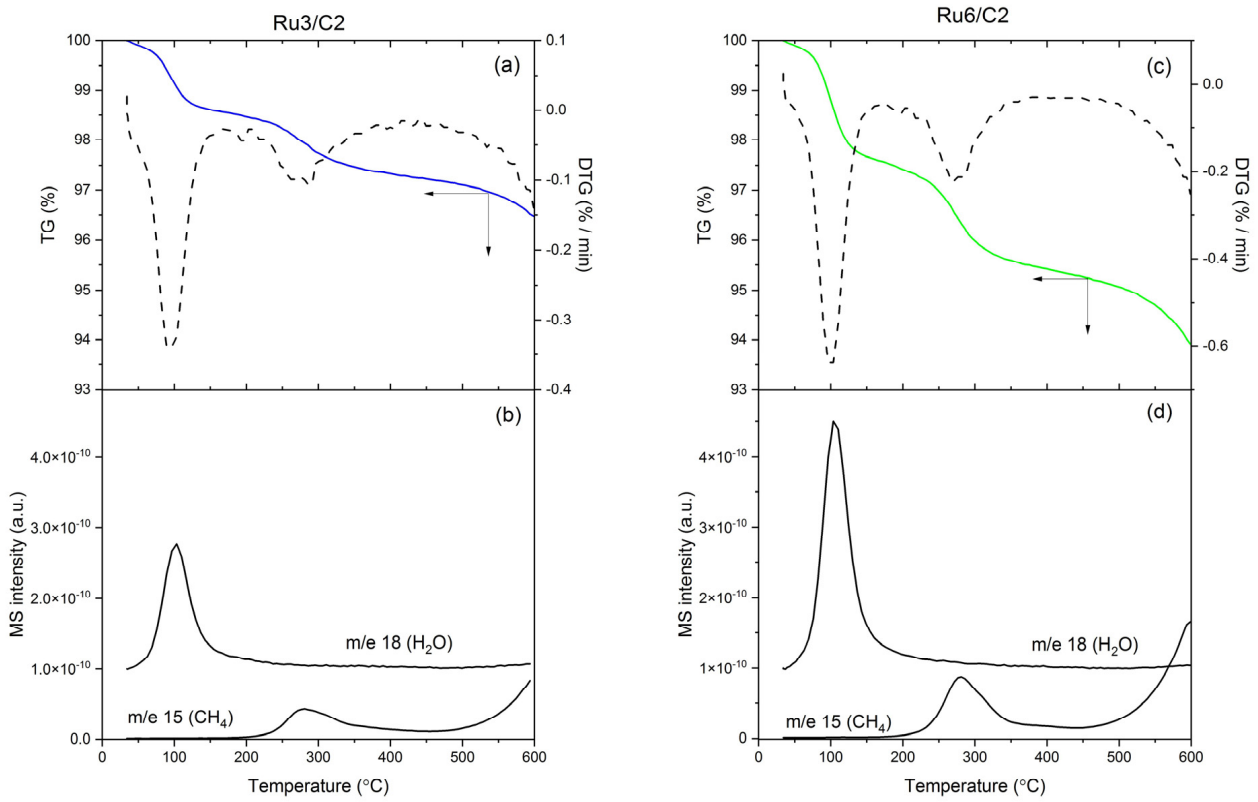


**Figure 9.** TG/DTG–MS profiles of the C2–supported catalysts: (**a**) Ru3/C2 mass loss during heating to 600 °C, (**b**) Ru3/C2 MS signal of water and methane evolution, (**c**) Ru6/C2 mass loss during heating to 600 °C, (**d**) Ru6/C2 MS signal of water and methane evolution.

The second of the recorded MS signals (m/e = 15) was registered to determine whether methanation of the carbon carrier took place during reduction. The MS m/e = 15 signals are visible in both samples (Figure 8b,d). The first one, at 250 °C, has similar intensiveness for both catalysts studied. It is probably related to the hydrogenation of the functional groups present on the surface of the support [27]. The second signal reaches a maximum at 360 °C. It is believed to correspond to the methanation of the carbon substrate in the vicinity of the Ru crystallites [36]. The signal is more intense for the Ru6/C1 sample, which may be related to the higher ruthenium content in the material. From around 400 °C, a slow increase in the amount of evolving methane begins. However, it should be noted that this is a negligible effect in comparison with the water signals. This may be related to the fact that some ruthenium crystallites form aggregates that are not bound to the carrier, as shown by the TEM results (Figures 3 and 4). Consequently, ruthenium has a limited ability to catalyze this undesirable reaction. In addition, the temperature operating range of CO methanation catalysts in industry is much lower than 400 °C [11]. Therefore, it can be concluded that C1–based systems are resistant to methanation under process conditions.

The course of reduction of C2–based catalysts is slightly different from that described for C1–supported catalysts. The recorded mass losses were 3.5 wt.% for Ru3/C2 (Figure 9a) and 6 wt.% for Ru6/C2 (Figure 9c). The DTG lines indicate better defined transformation stages. Similar to the samples supported on carbon C1, water release is observed (Figure 9b,d), with a maximum at around 120 °C. It is noteworthy that this is a sharp, narrow signal. This is probably due to the high homogeneity of the size of the particles undergoing reduction, which was confirmed by both the results based on the CO chemisorption (Table 1) and the TEM images (Figures 5 and 6). Also, the fact that water formation

was no longer observed downstream supports this explanation. It is also worth noting, that the water release signal at around 120 °C has a much higher intensity than that obtained for the C1–based samples (Figure 8). This, in turn, may be related to the higher amount of water adsorbed on the more developed surface of C2 carbon and, also, to the higher proportion of the oxide layer covering the ruthenium particles, which undergoes reduction. As can be seen from the TEM images shown in Figures 5 and 6, the thickness of the oxide layer is higher the smaller the ruthenium crystallites. And this is precisely the relationship we observe when comparing samples supported on C2 with those on C1.

Two effects are observed on the MS line m/e = 15 (Figure 9b,d), corresponding to methane release. A clear signal of $CH_4$ formation was obtained at around 275 °C. It has a higher intensity for the Ru6/C2 sample than the Ru3/C2 sample. It seems that similar to what was described earlier, it comes from the hydrogenation of the functional groups on the carrier, and the increase in its intensity is related to the higher ruthenium content in the sample. An interesting effect is observed starting at a temperature of about 450 °C. A steady, rapid increase in the amount of methane was registered. It should be attributed to the methanation of the support, which occurs more intensely for higher ruthenium loading in the sample. This can also be seen in the marked decrease in the TG line (Figure 9a,c). As described earlier, the industrial conditions of catalytic CO methanation are below 400 °C. Therefore, it can be assumed that C2–based systems are also resistant to methanation. Two main reasons behind the different behavior of C2–based samples relative to those based on C1 can be identified. The first is that the Ru crystallites are much smaller, at the same loading, and remain in closer contact with the support, as evidenced by the TEM results. The second reason is due to the carbon carrier. The C2 carbon, which has a more developed specific surface area due to gasification in steam, is more easily methanized in the presence of ruthenium [23,36].

### *2.7. CO–TPD*

Carbon monoxide desorption studies were performed to characterize the chemical nature of the ruthenium/carbon catalyst surface. The obtained profiles for the fresh and spent catalysts are presented in Figure 10.

As shown in Figure 10, the way CO interacted with the surface of the tested catalysts differed primarily depending on the carrier used. For samples supported on carbon C1, the amounts of desorbing CO were about an order of magnitude smaller than for samples supported on C2. For fresh samples deposited on carbon C1 (Figure 10a,b), a broad peak with a maximum temperature in the 140–150 °C range is observed, followed by two sharp signals at temperatures above 500 °C, resulting from the desorption of the functional groups present on the support surface (Figure S3). The intensities of the individual signals were similar for both samples, regardless of the Ru content in the sample. The long–term stability tests did not change the position of the first peak, while there were some shifts in the positions of the high–temperature peaks. There was also a slight decrease in the amount of CO desorbing from the surface of the catalysts after the tests.

For samples deposited on C2 carbon, two strong CO desorption peaks were obtained at 150–260 °C for Ru3/C2 (Figure 10c) and 160–270 °C for Ru6/C2 (Figure 10d). The shape and ratio of these two signals were preserved in the post–test samples, although the former shifted toward lower temperatures for both Ru3/C2 and Ru6/C2 (Figure 10c,d). A very pronounced decrease in their intensity was observed for the post–test samples. This is associated with a significant reduction in the number of adsorption sites on the surface of the catalysts after operation or a significant change in their structure [4]. Another possible reason was described by Panagiotopoulou [45]. The authors reported [45] that only a small part of CO preadsorbed on the (5 wt.%) $Ru/TiO_2$ ($d_{Ru}$ = 4.5 nm) catalyst desorbed during the TPD experiment in its molecular form. The authors claim that the largest amount of adsorbed CO species participates in surface reactions upon heating under He flow and yields $CO_2$ in the gas phase due to the Boudouard reaction or WGS reaction [45]. Therefore, it is supposed that ruthenium particles of different sizes interact differently with

the adsorbed CO, giving different TPD–CO profiles [45]. Moreover, Reed claimed [46] that the adsorption properties of the ruthenium surface are very sensitive to the presence of carbon. Therefore, the obtained TPD profiles are related not only to the carbon deposition (spent catalysts), but also to the presence of carbon functional groups on the surface of fresh samples, according to which the amount depends on the used carrier [47]. The resulting picture of the CO interaction with the surface of Ru/carbon–based systems (Figure 10) does not allow a clear link to activity in CO methanation. It is supposed that the structure of the active sites must play a key role in shaping the activity of the catalysts. At this stage of our research, it is impossible to indicate the clear reason for the observed activity trends. However, it must be noted that prepared ruthenium catalysts exhibited high activity and stability, which makes them promising from an application point of view.

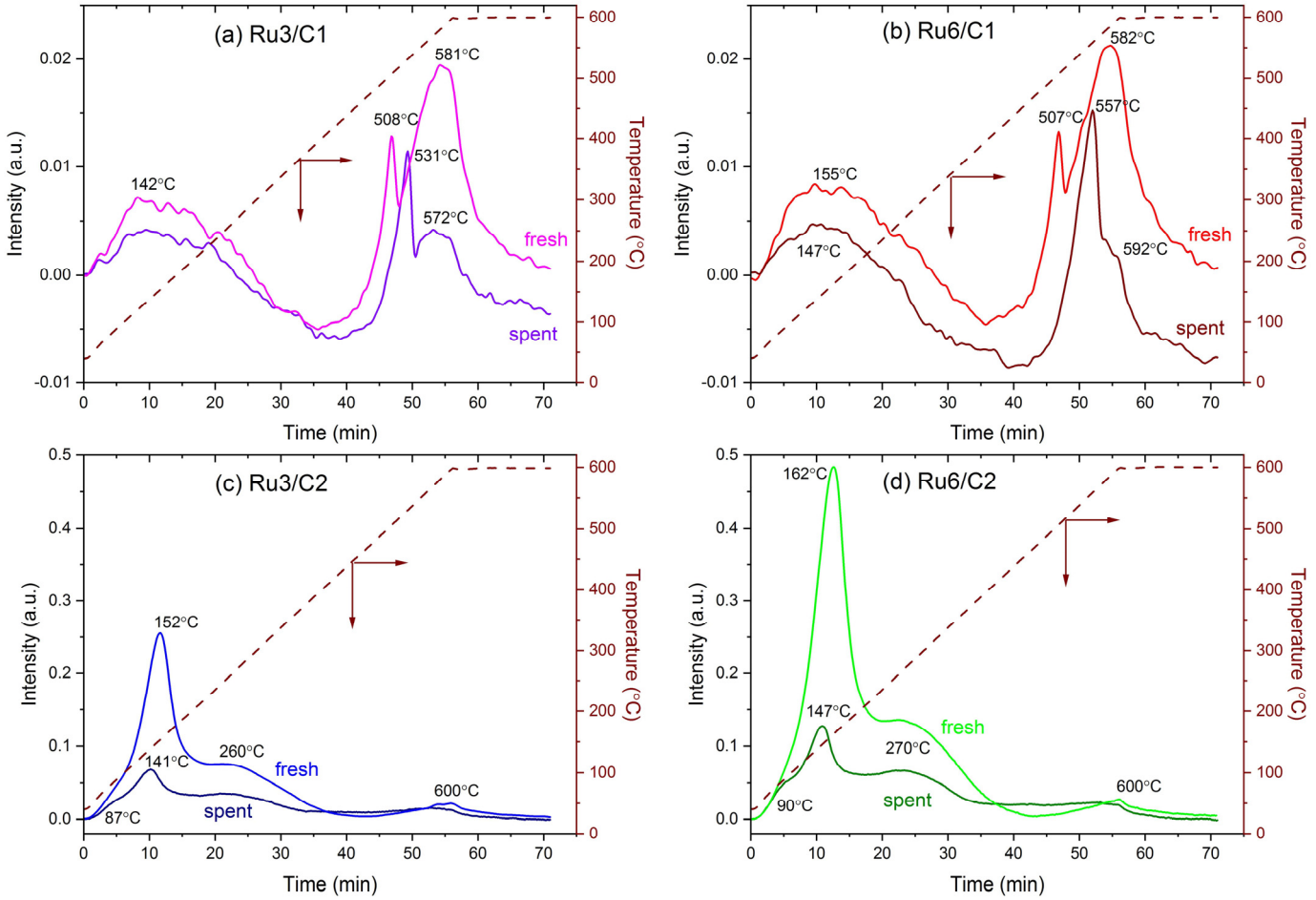


**Figure 10.** CO–TPD profiles of the fresh and spent Ru/C catalysts: (**a**) Ru3/C1; (**b**) Ru6/C1; (**c**) Ru3/C2; (**d**) Ru6/C2.

## 3. Materials and Methods

### *3.1. Catalysts Synthesis*

Carbon supports used in this study were obtained from commercial active carbon GF40 (Norit B.V. Company, Amersfoort, The Netherlands). A batch of this material was preheated for 2 h at 1900 °C in a protected argon atmosphere. The obtained carbon support, with a surface area of 23 $m^2/g$, was marked as C1. In the next step, a part of the C1 material was gasified for 5 h with the $H_2O$ + Ar stream (50 vol.% of $H_2O$ in the mixture) at 856 °C. Consequently, it lost 25% of its mass, but the obtained material, marked as C2, exhibited a very large surface area equal to 1457 $m^2/g$. This is in accordance with [48,49] that partial gasification, performed in the case of C2 preparation, enabled partial recovery of the porosity lost in the first step of thermal treatment, which is responsible for the large surface

area. Weighed portions of whole grains of carbon materials were then impregnated with an acetone solution of the ruthenium precursor ($RuCl_3 \cdot 0.5\ H_2O$, Sigma Aldrich, Darmstadt, Germany). A wet impregnation procedure [26] was used to introduce the appropriate amount of ruthenium salt to obtain 3 or 6 wt.% Ru loading in the final Ru/carbon system. The impregnated materials were dried for 24 h at 90 °C, reduced in flowing hydrogen and passivated, according to the procedure described in [26]. Four catalysts: Ru3/C1, Ru6/C1, Ru3/C2 and Ru6/C2 were obtained. Their symbols specify the Ru wt.% loading and proper carbon support.

### *3.2. Characterization Studies*

The specific surface area of C1 and C2 carbon supports was determined by nitrogen adsorption at −196 °C. Before analysis with the use of an ASAP 2020 instrument (Micromeritics) [50], the samples were degassed (vacuum, 1 h at 90 °C, plus 4 h at 300 °C).

Conventional CO chemisorption volumetric experiments, described in [26], were performed for the fresh and spent catalysts using an ASAP 2020 instrument (Micromeritics). The samples (mass 0.2 g, fraction 0.2 ÷ 0.63 mm) were reduced in hydrogen flow (80 $cm^3$/min) at 420 °C for 10 h. After flushing with helium at 420 °C for 2 h, the samples were cooled to 35 °C and exposed to carbon monoxide in the pressure range 6.7–60 kPa.

Powder X–ray diffraction patterns were recorded on a Bruker D8 Advance diffractometer operating with Cu–Kα radiation (λ = 0.154 nm) and equipped with a LynxEye position sensitive detector [50]. Experiments were performed for powdered fresh catalysts. Data were collected in the Bragg–Brentano geometry within the 2θ angle range 10–90° with step 0.03°, 10 s/step at room temperature. The Scherrer equation [51] (k = 0.89) was used to calculate the average Ru crystallite sizes in the samples.

TEM images were recorded for powdered samples of fresh and spent catalysts, with a Philips CM20 Super Twin microscope. A detailed description of the experimental procedure can be found in [25].

The disorder in the carbon supports structure was characterized in selected samples with Raman spectroscopy [44]. The powdered fresh materials and spent catalysts were characterized using a Renishaw inVia Qontor confocal Raman microscope. The excitation wavelength was 532 nm from a 45 W laser with an 1800 $nm^{-1}$ grating as the light source. The measurement detail parameters can be found in [44].

The TG–MS experiments were performed using a thermogravimetric analyzer (TGA, NETZSCH STA449C) coupled with a mass spectrometer NETZSCH QMS Aëolos 403C. The powdered catalyst samples (0.02 g) were loaded onto alumina plates and heated up to 600 °C, with a constant rate of 10 °C/min in the $H_2$ + Ar stream (50 vol.% $H_2$/Ar mixture, 100 $cm^3$/min). The mass change, temperature and selected m/e signals were monitored during the whole experiment. To avoid water condensation, all the necessary apparatus parts were kept heated to 250 °C.

The CO–TPD measurements were performed for both the fresh and spent catalysts. A sample (mass 0.2 g, fraction 0.2 ÷ 0.63 mm) was loaded into a U–shaped quartz reactor and connected with an AutoChem II 2920 (Micromeritics) chemisorption analyzer. After 10 h of reduction at 400 °C in the $H_2$ flow (40 $cm^3$/min), the gas flow was switched to helium for purging at 430 °C for 1 h. The CO adsorption was carried out at 40 °C for 2 h in the CO/He mixture flow (90 vol.% CO in He, 40 $cm^3$/min). Next, the sample was rinsed with helium at 40 °C for 1 h to remove physisorbed carbon monoxide and heated up to 600 °C in the helium flow at a ramping rate of 10 °C/min. The final temperature was maintained for 15 min. The outlet gas was analyzed by a thermal conductivity detector (TCD).

### *3.3. Catalytic Activity Studies*

The long–term stability of the prepared Ru/carbon catalysts in CO methanation was tested in a setup described in [26] under atmospheric pressure. A model, simplified gas mixture, containing 5000 ppm CO in $H_2$ was used for the activity tests. The precise and stable composition of the inlet gas stream was made possible by using mass–flow controllers.

Small samples of the Ru/carbon catalysts (0.25 g, fraction 0.2 ÷ 0.63 mm) were activated in flowing $H_2$ (40 $cm^3$/min) at 400 °C for 18 h. Then, the reactor was cooled to 270 °C, and the gas stream was switched to a CO + $H_2$ mixture (total gas flow 80 $cm^3$/min). After 1 h of stabilization at the desired temperature (270–240–220 °C), the outlet gas composition was monitored with a gas chromatograph (Trace 1310, Thermo Scientific, Waltham, MA, USA) equipped with a $CO_x$ methanizer and a flame ionization detector. The deviation of the GC data was within 2%. The total conversion of carbon monoxide was calculated on the basis of its inlet–outlet mass balance. The activity of four tested catalysts was compared on the basis of the reaction rate of CO methanation, normalized to the same Ru weight in the sample. That value was calculated from the CO conversion, the inlet molar flow rate of CO and the mass of Ru in the sample.

The procedure for time–on–stream tests was as follows: after the last tests at 220 °C, the sample was overheated at 300 °C in the CO + $H_2$ (5000 ppm CO in $H_2$) gas mixture (80 $cm^3$/min) for 24 h (or 72 h during the weekend) at 0.1 MPa. It was cyclically repeated for 9 working days, which gives a total time on stream test duration of 240 h.

## 4. Conclusions

The influence of the long–term exploitation of Ru/C materials during CO methanation on the textural and structural properties and their catalytic behavior have been investigated. C1–supported catalysts were less active than their C2–supported counterparts. For two samples based on the same carbon support, higher activities were observed for lower ruthenium loadings. The most favorable catalytic performance was achieved with the Ru3/C2 catalyst. Three of the prepared samples, i.e., Ru3/C2, Ru6/C2 and Ru3/C1 catalysts, were revealed to be strongly resistant to overheating and exhibited stable activity for over 240 h. We have also shown that the introduction of ruthenium onto the support surface and stability tests performed resulted in structural changes in the carbon material. The observed changes can be attributed to carbon deposition, which was especially well detected in samples with low Ru dispersion. It was revealed that Ru/carbon materials were resistant to the undesired reaction of carbon support methanation under industrially relevant conditions. The type of carbon support and ruthenium dispersion substantially affected the amounts of CO adsorbed on the Ru surface and the way its chemical transformation occurred on the catalyst's surface. It is supposed that these factors determine the amount and nature of the Ru active sites. These findings clearly indicate the need for further research concerning the structure of active sites existing on different ruthenium surfaces in supported systems. The present observations can contribute to designing highly active, stable catalysts for hydrogen purification.

**Supplementary Materials:** The following supporting information can be downloaded at: https://www.mdpi.com/article/10.3390/catal13121518/s1, Figure S1: CO conversion changes during time of stream tests on the Ru/carbon catalysts: (a) 270 °C, (b) 240 °C and (c) 220 °C; measurement conditions: 0.1 MPa, 5000 ppm CO in CO–$H_2$ mixture, 80 $cm^3$/min; overheating conditions: 300 °C, 0.1 MPa, 5000 ppm CO in CO–$H_2$ mixture, 80 $cm^3$/min; Figure S2: XRPD patterns of the carbon supports used for Ru/carbon systems preparation; Table S1: Full width at half the maximum of the D (ΓD) and G (ΓG) bands and position of the G peak (ωG) in Raman spectra; Figure S3: CO–TPD profiles of the two carbon supports used in the study.

**Author Contributions:** Conceptualization, E.T.; Data curation, E.T., K.L., M.O., A.O. and L.K.; Formal analysis, E.T., M.O., A.O. and L.K.; Funding acquisition, E.T.; Investigation, E.T., K.L., M.O., A.O. and L.K.; Methodology, E.T., M.O., A.O. and L.K.; Project administration, E.T.; Resources, E.T.; Supervision, E.T.; Validation, E.T., M.O. and L.K.; Visualization, E.T., M.O., A.O. and L.K.; Writing—original draft, E.T.; Writing—review and editing, E.T., M.O. and L.K. All authors have read and agreed to the published version of the manuscript.

**Funding:** This work was supported by the Warsaw University of Technology under I–Chem.4 project of the Scientific Council for Chemical Engineering.

**Data Availability Statement:** Data are contained within the article.

**Conflicts of Interest:** The authors declare no conflict of interest. The funders had no role in the design of the study; in the collection, analyses, or interpretation of data; in the writing of the manuscript; or in the decision to publish the results.

## References


1. Argyle, M.D.; Bartholomew, C.H. Heterogeneous Catalyst Deactivation and Regeneration: A Review. *Catalysts* **2015**, *5*, 145–269. [CrossRef]
2. Alihosseinzadeh, A.; Nematollahi, B.; Rezaei, M.; Lay, E.N. CO methanation over Ni catalysts supported on high surface area mesoporous nanocrystalline γ-$Al_2O_3$ for CO removal in $H_2$-rich stream. *Int. J. Hydrogen Energy* **2015**, *40*, 1809–1819. [CrossRef]
3. Abdel-Mageed, A.M.; Widmann, D.; Olesen, S.E.; Chorkendorff, I.; Behm, R.J. Selective CO Methanation on Highly Active Ru/$TiO_2$ Catalysts: Identifying the Physical Origin of the Observed Activation/Deactivation and Loss in Selectivity. *ACS Catal.* **2018**, *8*, 5399–5414. [CrossRef]
4. Chen, S.; Abdel-Mageed, A.M.; Li, D.; Bansmann, J.; Cisneros, S.; Biskupek, J.; Huang, W.; Behm, R.J. Morphology-Engineered Highly Active and Stable Ru/$TiO_2$ Catalysts for Selective CO Methanation. *Angew. Chem. Int. Ed.* **2019**, *58*, 10732–10736. [CrossRef]
5. Dai, X.; Liang, J.; Ma, D.; Zhang, X.; Zhao, H.; Zhao, B.; Guo, Z.; Kleitz, F.; Qiao, S. Large-pore mesoporous RuNi-doped $TiO_2$-$Al_2O_3$ nanocomposites for highly efficient selective CO methanation in hydrogen-rich reformate gases. *Appl. Catal. B Environ.* **2015**, *165*, 752–762. [CrossRef]
6. Munnik, P.; Velthoen, M.E.Z.; de Jongh, P.E.; de Jong, K.P.; Gommes, C.J. Nanoparticle Growth in Supported Nickel Catalysts during Methanation Reaction-Larger is Better. *Angew. Chem. Int. Ed.* **2014**, *53*, 9493–9497. [CrossRef]
7. Grams, J.; Ruppert, A.M. Catalyst Stability—Bottleneck of Efficient Catalytic Pyrolysis. *Catalysts* **2021**, *11*, 265. [CrossRef]
8. Gao, J.; Wang, Y.; Ping, Y.; Hu, D.; Xu, G.; Gu, F.; Su, F. A thermodynamic analysis of methanation reactions of carbon oxides for the production of synthetic natural gas. *RSC Adv.* **2012**, *2*, 2358–2368. [CrossRef]
9. Garbarino, G.; Bellotti, D.; Riani, P.; Magistri, L.; Busca, G. Methanation of carbon dioxide on Ru/$Al_2O_3$ and Ni/$Al_2O_3$ catalysts at atmospheric pressure: Catalysts activation, behaviour and stability. *Int. J. Hydrogen Energy* **2015**, *40*, 9171–9182. [CrossRef]
10. Pena, M.A.; Gómez, J.P.; Fierro, J.L.G. New catalytic routes for syngas and hydrogen production. *Appl. Catal. A Gen.* **1996**, *144*, 7–57. [CrossRef]
11. Tada, S.; Kikuchi, R. Mechanistic Study and Catalyst Development for Selective Carbon Monoxide Methanation. *Catal. Sci. Technol.* **2015**, *5*, 3061–3070. [CrossRef]
12. Garbis, P.; Jess, A. Selective CO methanation in $H_2$-rich gas for household fuel cell applications. *Energies* **2020**, *13*, 2844. [CrossRef]
13. Méndez-Mateos, D.; Barrio, V.L.; Requies, J.M.; Cambra, J.F. Effect of the Addition of Alkaline Earth and Lanthanide Metals for the Modification of the Alumina Support in Ni and Ru Catalysts in $CO_2$ Methanation. *Catalysts* **2021**, *11*, 353. [CrossRef]
14. Gao, J.; Liu, Q.; Gu, F.; Liu, B.; Zhong, Z.; Su, F. Recent advances in methanation catalysts for the production of synthetic natural gas. *RSC Adv.* **2015**, *5*, 22759–22776. [CrossRef]
15. Chen, S.; Abdel-Mageed, A.M.; Dyballa, M.; Parlinska-Wojtan, M.; Bansmann, J.; Pollastri, S.; Olivi, L.; Aquilanti, G.; Behm, R.J. Raising the $CO_x$ Methanation Activity of a Ru/γ-$Al_2O_3$ Catalyst by Activated Modification of Metal–Support Interactions. *Angew. Chem. Int. Ed.* **2020**, *59*, 22763–22770. [CrossRef]
16. Eckle, S.; Anfang, H.G.; Behm, R.J. What drives the selectivity for CO methanation in the methanation of $CO_2$-rich reformate gases on supported Ru catalysts? *Appl. Catal. A Gen.* **2011**, *391*, 325–333. [CrossRef]
17. Panagiotopoulou, P.; Kondarides, D.I.; Verykios, X.E. Selective methanation of CO over supported Ru catalysts. *Appl. Catal. B Environ.* **2009**, *88*, 470–478. [CrossRef]
18. Chen, S.; Abdel-Mageed, A.M.; Gauckler, C.; Olesen, S.E.; Chorkendorff, I.; Behm, R.J. Selective CO methanation on isostructural Ru nanocatalysts: The role of support effects. *J. Catal.* **2019**, *373*, 103–115. [CrossRef]
19. Zhang, Y.; Zhang, G.; Wang, L.; Xu, Y.; Sun, Y. Selective methanation of carbon monoxide over Ru-based catalysts in $H_2$-rich gases. *J. Ind. Eng. Chem.* **2012**, *18*, 1590–1597. [CrossRef]
20. Xiong, J.; Dong, X.; Li, L. CO selective methanation in hydrogen-rich gas mixtures over carbon nanotube supported Ru-based catalysts. *J. Nat. Gas Chem.* **2012**, *21*, 445–451. [CrossRef]
21. Kumi, D.O.; Phaahlamohlaka, T.N.; Dlamini, M.W.; Mangezvo, I.T.; Mhlanga, S.D.; Scurrell, M.S.; Coville, N.J. Effect of a titania covering on CNTS as support for the Ru catalysed selective CO methanation. *Appl. Catal. B Environ.* **2018**, *232*, 492–500. [CrossRef]
22. Kumi, D.O.; Dlamini, M.W.; Phaahlamohlaka, T.N.; Mhlanga, S.D.; Coville, N.J.; Scurrell, M.S. Selective CO Methanation Over Ru Supported on Carbon Spheres: The Effect of Carbon Functionalization on the Reverse Water Gas Shift Reaction. *Catal. Lett.* **2018**, *148*, 3502–3513. [CrossRef]
23. Truszkiewicz, E.; Bielecka, A.; Moszyński, D.; Ostrowski, A. Lowering risk of methanation of carbon support in Ru/carbon catalysts for CO methanation by adding lanthanum. *Int. J. Hydrogen Energy* **2023**, *48*, 24936–24950. [CrossRef]
24. Lederhos, C.R.; L'Argentière, P.C.; Coloma-Pascual, F.; Fígoli, N.S. A study about the effect of the temperature of hydrogen treatment on the properties of Ru/$Al_2O_3$ and Ru/C and their catalytic behavior during 1-heptyne semi-hydrogenation. *Catal. Lett.* **2006**, *110*, 23–28. [CrossRef]
25. Truszkiewicz, E.; Zegadło, K.; Wojda, D.; Mierzwa, B.; Kępiński, L. The effect of the ruthenium crystallite size on the activity of Ru/carbon systems in CO methanation. *Top. Catal.* **2017**, *60*, 1299–1305. [CrossRef]

26. Truszkiewicz, E.; Kowalczyk, K.; Dębska, A.; Wojda, D.; Iwanek, E.; Kępiński, L.; Mierzwa, B. Methanation of CO on Ru/graphitized-carbon catalysts: Effects of the preparation method and the carbon support structure. *Int. J. Hydrogen Energy* **2020**, *45*, 31985–31999. [CrossRef]
27. Guo, X.; Dong, H.; Li, B.; Dong, L.; Mu, X.; Chen, X. Influence of the functional groups of multiwalled carbon nanotubes on performance of Ru catalysts in sorbitol hydrogenolysis to glycols. *J. Mol. Catal. A Chem.* **2017**, *426*, 79–87. [CrossRef]
28. Kowalczyk, Z.; Stolecki, K.; Raróg-Pilecka, W.; Miśkiewicz, E.; Wilczkowska, E.; Karpiński, Z. Catalytic properties of small ruthenium particles supported on carbon. Studies of carbon monoxide methanation. *Pol. J. Chem.* **2008**, *82*, 607.
29. Eckle, S.; Denkwitz, Y.; Behm, R.J. Activity, selectivity, and adsorbed reaction intermediates/reaction side products in the selective methanation of CO in reformate gases on supported Ru catalysts. *J. Catal.* **2010**, *269*, 255–268. [CrossRef]
30. Borodziński, A.; Bonarowska, M. Relation between Crystallite Size and Dispersion on Supported Metal Catalysts. *Langmuir* **1997**, *13*, 5613–5620. [CrossRef]
31. Chen, K.; Li, Y.; Wang, M.; Wang, Y.; Cheng, K.; Zhang, Q.; Kang, J.; Wang, Y. Functionalized Carbon Materials in Syngas Conversion. *Small* **2021**, *17*, 2007527. [CrossRef] [PubMed]
32. Abdel-Mageed, A.M.; Widmann, D.; Olesen, S.E.; Chorkendorff, I.; Biskupek, J.; Behm, R.J. Selective CO Methanation on Ru/$TiO_2$ Catalysts: Role and Influence of Metal-Support Interactions. *ACS Catal.* **2015**, *5*, 6753–6763. [CrossRef]
33. Mieth, J.A.; Schwarz, J.A. The effect of catalyst preparation on the performance of alumina-supported ruthenium catalysts I. The impact of catalytic precursor on particle size and catalytic activity. *J. Catal.* **1989**, *118*, 203–217. [CrossRef]
34. Dagle, R.A.; Wang, Y.; Xia, G.G.; Strohm, J.J.; Holladay, J.; Palo, D.R. Selective CO methanation catalysts for fuel processing applications. *Appl. Catal. A Gen.* **2007**, *326*, 213–218. [CrossRef]
35. Jang, H.; Kim, S.H.; Lee, D.; Shim, S.E.; Baeck, S.H.; Kim, B.S.; Chang, T.S. Hydrogenation of lactic acid to propylene glycol over a carbon-supported ruthenium catalyst. *J. Mol. Catal. A Chem.* **2013**, *380*, 57–60. [CrossRef]
36. Iost, K.N.; Borisov, V.A.; Temerev, V.L.; Smirnova, N.S.; Surovikin, Y.V.; Trenikhin, M.V.; Arbuzov, A.B.; Gulyaeva, T.I.; Shlyapin, D.A.; Tsyrulnikov, P.G.; et al. Effect of the carbon support graphitization on the activity and thermal stability of Ru-Ba-Cs/C ammonia decomposition catalysts. *React. Kinet. Mech. Catal.* **2019**, *127*, 85–102. [CrossRef]
37. Bartholomew, C.H. Mechanisms of catalyst deactivation. *Appl. Catal. A Gen.* **2001**, *212*, 17–60. [CrossRef]
38. Moodley, D.J.; van de Loosdrecht, J.; Saib, A.M.; Overett, M.J.; Datye, A.K.; Niemantsverdriet, J.W. Carbon deposition as a deactivation mechanism of cobalt-based Fischer–Tropsch synthesis catalysts under realistic conditions. *Appl. Catal. A Gen.* **2009**, *354*, 102–110. [CrossRef]
39. Bartholomew, C.H. Carbon Deposition in Steam Reforming and Methanation. *Catal. Rev.* **1982**, *24*, 67–112. [CrossRef]
40. Olesen, S.E.; Andersson, K.J.; Damsgaard, C.D.; Chorkendorff, I. Deactivating Carbon Formation on a Ni/$Al_2O_3$ Catalyst under Methanation Conditions. *J. Phys. Chem. C* **2017**, *121*, 15556–15564. [CrossRef]
41. Ferrari, A.C. Raman spectrum of graphene and graphene layers. *Solid State Commun.* **2007**, *143*, 47–57. [CrossRef]
42. Ferrari, A.; Robertson, J. Interpretation of Raman spectra of disordered and amorphous carbon. *Phys. Rev. B—Condens. Matter Mater. Phys.* **2000**, *61*, 14095–14107. [CrossRef]
43. Yoshida, A.; Kaburagi, Y.; Hishiyama, Y. Full width at half maximum intensity of the G band in the first order Raman spectrum of carbon material as a parameter for graphitization. *Carbon N. Y.* **2006**, *44*, 2333–2335. [CrossRef]
44. Truszkiewicz, E.; Bielecka, A.; Iwanek (nee Wilczkowska), E.M.; Ojrzyńska, M.; Ostrowski, A. CO Removal from Hydrogen Stream through Methanation on Ru/C Catalysts Doped with Lanthanum and Barium. *Hydrogen* **2023**, *4*, 389–407. [CrossRef]
45. Panagiotopoulou, P.; Kondarides, D.I.; Verykios, X.E. Mechanistic study of the selective methanation of CO over Ru/TiO 2 catalyst: Identification of active surface species and reaction pathways. *J. Phys. Chem. C* **2011**, *115*, 1220–1230. [CrossRef]
46. Reed, P.D.; Comrie, C.M.; Lambert, R.M. Chemisorption, surface structural chemistry, and electron impact properties of carbon monoxide on Ru(101). *Surf. Sci.* **1976**, *59*, 33–45. [CrossRef]
47. Lin, B.; Guo, Y.; Cao, C.; Ni, J.; Lin, J.; Jiang, L. Carbon support surface effects in the catalytic performance of Ba-promoted Ru catalyst for ammonia synthesis. *Catal. Today* **2018**, *316*, 230–236. [CrossRef]
48. Kowalczyk, Z.; Sentek, J.; Jodzis, S.; Mizera, E.; Góralski, J.; Paryjczak, T.; Diduszko, R. An alkali-promoted ruthenium catalyst for the synthesis of ammonia, supported on thermally modified active carbon. *Catal. Lett.* **1997**, *45*, 65–72. [CrossRef]
49. Raróg-Pilecka, W.; Miśkiewicz, E.; Szmigiel, D.; Kowalczyk, Z. Structure sensitivity of ammonia synthesis over promoted ruthenium catalysts supported on graphitised carbon. *J. Catal.* **2005**, *231*, 11–19. [CrossRef]
50. Ronduda, H.; Zybert, M.; Patkowski, W.; Ostrowski, A.; Jodłowski, P.; Szymański, D.; Kępiński, L.; Raróg-Pilecka, W. Boosting the catalytic performance of co/mg/la catalyst for ammonia synthesis by selecting a pre-treatment method. *Catalysts* **2021**, *11*, 941. [CrossRef]
51. Jiménez, V.; Sánchez, P.; Panagiotopoulou, P.; Valverde, J.L.; Romero, A. Methanation of CO, $CO_2$ and selective methanation of CO, in mixtures of CO and $CO_2$, over ruthenium carbon nanofibers catalysts. *Appl. Catal. A Gen.* **2010**, *390*, 35–44. [CrossRef]